Kinetic Modeling of Phototrophic Biofilms: The PHOBIA Model

Gundula Wolf, Cristian Picioreanu, Mark C.M. van Loosdrecht

Department of Biotechnology, Delft University of Technology, Julianalaan 67, 2628 BC Delft, The Netherlands; telephone: +31-(0)15-278-1618; fax: +31-(0)15-278-2355; e-mail: m.c.m.vanloosdrecht@tudelft.nl

ABSTRACT: A kinetic model for mixed phototrophic biofilms is introduced, which focuses on the interactions between photoautotrophic, heterotrophic, and chemoautotrophic (nitrifying) functional microbial groups. Biofilm-specific phenomena are taken into account, such as extracellular polymeric substances (EPS) production by phototrophs as well as gradients of substrates and light in the biofilm. Acid–base equilibria, in particular carbon speciation, are explicitly accounted for, allowing for the determination of pH profiles across the biofilm. Further to previous models reported in literature, the PHOBIA model combines a number of kinetic mechanisms specific to phototrophic microbial communities, such as internal polyglucose storage under dynamic light conditions, phototrophic growth in the darkness using internally stored reserves, photoadaptation and photoinhibition, preference for ammonia over nitrate as N-source and the ability to utilize bicarbonate as a carbon source in the absence of CO_2. The sensitivity of the PHOBIA model to a number of key parameters is analyzed. An example on the potential use of phototrophic biofilms in wastewater polishing is discussed, where their performance is compared with conventional algal ponds. The PHOBIA model is presented in a manner that is compatible with other reference models in the area of water treatment. Its current version forms a theoretical base which is readily extendable once further experimental observations become available.

Biotechnol. Bioeng. 2007;97: 1064–1079.

© 2007 Wiley Periodicals, Inc.

KEYWORDS: phototrophic biofilm; model; EPS; pH; internal storage; carbon speciation

Introduction

Phototrophic biofilms can generally be described as light-driven microbial communities, which are attached to a solid support (substratum). They are omnipresent in nature, and they play an important ecological role in the elemental cycling of carbon and nutrients by performing CO_2 reduction and nitrogen fixation. Some phototrophic biofilms can be detrimental, for example, in biofouling of ship hulls. However, they can be advantageous in environmental engineering applications. They may, for example, be utilized in polishing nutrient-containing effluents from wastewater treatment installations, which are generally poor in organic carbon (Schumacher and Sekoulov, 2003). Furthermore, they were reported to aid in water disinfection (Schumacher and Sekoulov, 2003) as well as heavy metal adsorption (Geesey and Jang, 1990). Another application includes their utilization for aquaculture and fish farming (van Dam et al., 2002).

Microbial communities in phototrophic biofilms exhibit distinct mechanisms that differ from those found in planktonic populations. Biofilm growth is promoted by the excretion of extracellular polymeric substances (EPS) by the cells. EPS serve as an adhesive agent enabling cellular attachment and form the biofilm matrix embedding the cells. Typically, concentration gradients of various dissolved chemical species (e.g., oxygen, substrates) occur across thick biofilms due to diffusional limitations, as well as light intensity gradients caused by the light absorption and scattering. These gradients cause the formation of ecological microniches in the biofilm. The microniches allow the simultaneous growth of different functional groups of microorganisms in mixed biofilms, such as photoautotrophs, chemoautotrophs, and heterotrophs, exhibiting aerobic, anoxic, or anaerobic metabolisms. Complex interactions between these groups take place, which may be of symbiosis or of competition-type. An example is the growth of heterotrophs on extracellular organic compounds excreted by phototrophs. The latter, in turn, may utilize the inorganic CO_2 produced in heterotrophic growth. Furthermore, aerobic chemoautotrophs, such as nitrifiers, may

benefit from photosynthesis-enhanced oxygen levels in deeper biofilm layers, while they simultaneously compete with the phototrophs for inorganic carbon.

This paper presents a kinetic model of interactions in mixed community phototrophic biofilms. Mathematical models of interactions between the microbial communities enable the study and explanation of complex key mechanisms that prevail in mixed phototrophic biofilms. Furthermore, a validated model is of great interest as it may aid in (a) identifying key strategies for controlling phototrophic biofilm growth, (b) optimizing phototrophic biofilms for engineered (bioremediation) applications, and (c) designing installations utilizing phototrophic biofilms, such as tertiary wastewater polishing systems.

Numerous models describing phototrophic microbial communities are documented in literature. Examples range from single-species (Barbosa et al., 2003; Wu and Merchuk, 2002) and multi-(phototrophic) species models (Huisman et al., 1999) to those of entire ecosystems, such as seas and oceans (Gregoire et al., 2004; Varela et al., 1995), estuaries (Duarte and Ferreira, 1997), rivers (Cloot and Pieterse, 1999; Reichert et al., 2001), or algal ponds (Jupsin et al., 2003). While all models include kinetic aspects of phototrophic communities, their focus and level of detail differ greatly depending on the context of the addressed system and on the prevailing environmental conditions. In the vast majority of the cases, planktonic systems were modeled. Models specifically dealing with phototrophic biofilms are scarce (as an example, see Flora et al., 1995) especially those focusing on mixed populations. In a natural system, however, mixed population biofilms are bound to occur and models representing the temporal development of such complex phototrophic communities are still missing.

The model presented in this study seeks to address this gap. It was developed within the frame of the EU project PHOBIA (see www.photobiofilms.org), in which the physiology of mixed phototrophic biofilms was studied using specifically designed incubators (Zippel and Neu, 2005). The kinetic and metabolic model, termed PHOBIA model henceforth, focuses on interactions between functional trophic groups, that is, heterotrophs, chemoautotrophs (nitrifiers), and photoautotrophs. In the first stage of PHOBIA model development, physiological phenomena from established planktonic models, such as photoadaptation and photoinhibition, light attenuation, as well as acid–base equilibria, were combined and implemented in the context of a biofilm. In the second stage, the model was extended by a number of important characteristic features in phototrophic biofilm systems, namely:

- speciation of ammonia (NH_3/NH_4^+) and inorganic carbon ($CO_2/HCO_3^-/CO_3^{2-}$) throughout the biofilm,
- calculation of pH profiles within the biofilm,
- explicit inclusion of kinetics of inorganic carbon utilization by autotrophs,
- ability of phototrophs to switch to bicarbonate as carbon source in the absence of carbon dioxide,

- growth of phototrophs on nitrate in case of ammonia depletion,
- formation of EPS by phototrophs,
- internal storage of polyglucose by phototrophs under alternating dark/light conditions,
- phototrophic growth in the darkness utilizing internally stored reserves,

The emphasis of this paper lies on describing the kinetic model, that is, its components, processes, parameters, and underlying assumptions. This is followed by a short discussion on parameter sensitivity and general trends that are identifiable with the model. The application of the model to the PHOBIA reactor case study is the subject of further publications (Staal et al., 2007).

The PHOBIA Model

The PHOBIA kinetic model is a multi-species and multi-substrate mechanistic biofilm model, which has been developed based on the general one-dimensional mathematical model described in Wanner and Gujer (1986) and Wanner and Reichert (1996) implemented in the AQUASIM 2.1 software (Reichert, 1998). All underlying transport phenomena are identical to those of the AQUASIM 2.1 biofilm compartment.

The state variables of the PHOBIA model are divided into concentrations of soluble (S_i) and particulate (X_i) matter, similarly to the approach used in other well-established aquatic models (e.g., Activated Sludge Models, Henze et al., 2000; River Water Quality Model, Reichert et al., 2001). A list of the model state variables is given in Table I. The variables X_{Het}, X_N, X_S and X_I, S_{O_2}, S_S, S_I are defined in analogy with the Activated Sludge Model. The remaining components are specific for the PHOBIA model, and an overview of their definitions is included in the Appendix.

The PHOBIA model takes biological and chemical conversion processes into account. Figure 1 gives a schematic overview of dynamic transformation processes and interactions between the different groups of microorganisms within the phototrophic biofilm system. The stoichiometry and kinetics of all model processes are provided in Table II (the acid–base reactions and their rate and dissociation constants), Table III (stoichiometry of biological processes), Table IV (rates of biological processes), and Table V (stoichiometry and rates of chemical processes).

Biological Conversion Processes

The biological processes in the model include biomass growth, biomass inactivation and lysis, substrate and nutrient conversion and production of internal and external storage compounds (Fig. 1).

Table I. Overview of state variables of the phobia model.

State variable	Unit	Definition	Reference model
Particulate components concentrations			
X_{PH}	kg COD/m^3	Phototrophic biomass	
X_N	kg COD/m^3	Autotrophic (nitrifying) biomass	ASM
X_{Het}	kg COD/m^3	Heterotrophic biomass	ASM
X_S	kg COD/m^3	Slowly degradable non-diffusible organic compounds	ASM
X_{PG}	kg COD/m^3	Internally stored polyglucose	
X_{EPS}	kg COD/m^3	Extracellular polymeric substances	
X_{EPSI}	kg COD/m^3	Inert extracellular polymeric substances	
X_I	kg COD/m^3	Inert organic compounds	ASM
Soluble components concentrations			
S_S	kg COD/m^3	Readily biodegradable organic compounds	ASM
S_I	kg COD/m^3	Inert soluble organic compounds arising in hydrolysis	ASM
$S_{I,PH}$	kg COD/m^3	Inert soluble organic compounds arising in inactivation of phototrophic biomass	
S_{CO_2}	kmol/m^3	Dissolved CO2	
S_{HCO_3}	kmol/m^3	Dissolved bicarbonate ion	
S_{CO_3}	kmol/m^3	Dissolved carbonate ion	
S_{NO_3}	kmol/m^3	Dissolved nitrate ion	
S_{NH_3}	kmol/m^3	Dissolved ammonia	
S_{NH_4}	kmol/m^3	Dissolved ammonium ion	
S_{O_2}	kmol/m^3	Dissolved oxygen	ASM
S_H	kmol/m^3	Hydrogen ion	

ASM = activated sludge models Henze et al. (2000).

The growth rate $r_{i,\text{growth}}$ of a microorganism i is commonly modeled by multiplying its maximum growth rate ($\mu_{\text{max},i} \cdot X_i$) with a number of limiting terms, which are specific for each microbial group, as in Equation (1):

$$r_{i,\text{growth}} = \mu_{\text{max},i} \cdot X_i \cdot \prod_j f_j \qquad (1)$$

The limitation terms f_j in Equation (1) may be of saturation (e.g., Monod-type kinetics), inhibition or optimum type.

In the PHOBIA model, a slightly different approach was followed. Instead of accounting for multiple simultaneous limitations, it is assumed that growth is limited by a single
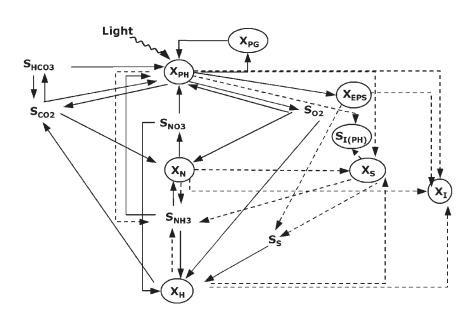

Figure 1. Conversion processes and interactions between different microbial groups in the phototrophic biofilm system. Full lines: Growth-related processes; broken lines: Biomass inactivation, lysis, and hydrolysis.

Table II. Acid–base reactions in the PHOBIA model and their rate and dissociation constants.

Reaction	pK_a (25°C)	Rate constant (25°C)	Source
$H_2O \rightleftarrows OH^- + H^+$	14	Implemented as equilibrium	Ebrahimi et al. (2003)
$CO_2 + H_2O \rightleftarrows HCO_3^- + H^+$	6.36	2,221 d^{-1}	Ebrahimi et al. (2003)
$CO_2 + OH^- \rightleftarrows HCO_3^-$ (relevant at pH > 10)	−7.64	10^{12} (very fast reaction)	Ebrahimi et al. (2003)
$HCO_3^- \rightleftarrows H^+ + CO_3^{2-}$	10.33	10^{12} (very fast reaction)	Ebrahimi et al. (2003)
$NH_4^+ \rightleftarrows NH_3 + H^+$	9.68	10^{12} (very fast reaction)	Musvoto et al. (2000)

substrate at a time see Equation (2):

$$r_{i,\text{growth}} = \mu_{\max,i} \cdot X_i \cdot \min(f_1, \ldots, f_j) \qquad (2)$$

The product term in Equation (1) results in a too low activity since the saturation terms for non-limiting substrates will be smaller than one. The growth rate of a microorganism based on Equation (2) is only depending on the truly limiting substrate, the advantages of using this approach is discussed in Bader (1978), Mankad and Nauman (1992), Ryder and Sinclair (1972), or dosSantos et al. (1996).

Heterotrophic and Chemoautotrophic Growth

Heterotrophic and chemoautotrophic (nitrifiers) growth were modeled as in ASM1 (Henze et al., 2000). Heterotrophic biomass was assumed to grow under aerobic as well as anoxic conditions (denitrification). For model simplification, both heterotrophic denitrification and chemoautotrophic nitrification were modeled as one-step processes, converting nitrate to N_2 and ammonia directly to nitrate, respectively.

Inactivation of Biomass

For each microbial group, a lumped process termed "inactivation" was implemented, representing the sum of all decay processes of that group. The inactivation process was modeled with first order kinetics for all three groups of microorganisms, based on the approach in ASM1 (Henze et al., 2000). The decay products are inert particulate organic substances X_I and slowly degradable particulate organic substance X_S. The latter is ultimately converted into readily degradable soluble COD by hydrolysis, and is available as substrate for the heterotrophic biomass. The third compound $S_{I,PH}$ is introduced in order to be able to balance the COD in the decay reaction of phototrophic biomass, because the elemental composition of the phototrophic biomass X_{PH} ($CH_{2.5}ON_{0.17}$) is assumed to be different from that of the heterotrophic (X_{Het}) and chemoautotrophic (X_N) biomass ($CH_{1.8}O_{0.5}N_{0.2}$). It is assumed that all three microbial groups degrade to the same X_S ($CH_{1.5}O_{0.5}N_{0.1}$) and X_I ($CH_{1.58}O_{0.5}N_{0.098}$) during inactivation.

Hydrolysis. Hydrolysis of organic compounds ensures that carbon-cycling takes place within the biofilm system through the conversion of slowly degradable organic material, such as EPS and particulate COD, into compounds readily utilizable by the heterotrophic biomass. The hydrolysis of slowly degradable particulate organic matter was implemented similar to ASM1 (Henze et al., 2000). For model simplification, hydrolysis was assumed to take place at the same rate irrespective of aerobic, anoxic, or anaerobic conditions. EPS hydrolysis describes the conversion of the EPS bound to the biofilm matrix. It is assumed that a fraction of the bound EPS is hydrolyzed in a simplified one-step reaction into soluble readily biodegradable COD (S_S), which can be utilized by heterotrophic biomass. The rest of the EPS remains in the system unchanged in the form of inert EPS ($X_{EPS,I}$). EPS hydrolysis kinetics was modeled as in (Horn et al., 2001), whereby it is assumed that the reaction only takes place when the concentration of S_S in the system is low. The stoichiometry of EPS hydrolysis was modeled as a function of the relative rate τ of soluble to inert EPS production.

Photoautotrophic Growth: Light Reactions

The growth metabolism of photoautotrophic microorganisms is dependent on the prevailing light regime. With light present as energy source, phototrophs carry out photosynthesis to convert inorganic carbon and water into oxygen and organic matter. Photosynthesis involves two main processes, that is, energy conversion and carbon fixation. In the energy conversion process, light energy is transformed into chemical energy, whereby oxygen is generated as a by-product. The carbon fixation mechanism then uses the energy stored to transform CO_2 to organic matter, for example, via the Calvin cycle involving the RubisCO enzyme. Besides converting inorganic CO_2 into biomass, phototrophs are able to channel part of the carbon either into internal polysaccharide reserves when exposed to alternating light regimes, or into EPS that are excreted in the surrounding environment. In the absence of general information on the kinetics of phototrophic EPS formation and internal polyglucose storage, the PHOBIA model assumes that both mechanisms are directly coupled to the microbial growth rate (Neu and Lawrence, 1997), that is, they exhibit the same kinetics (Horn et al., 2001).

The stoichiometry of phototrophic growth was expressed as a function of two relative rates ϕ and ε, relating to the mass of internal polyglucose produced and EPS formed, respectively, relative to the amount of phototrophic biomass

Table III. Stoichiometry table of the biological processes in the PHOBIA model.

Process		Particulates										Solubles					Rates
	X_{PH} kg$_{COD}$ m^{-3}	X_N kg$_{COD}$ m^{-3}	X_{Het} kg$_{COD}$ m^{-3}	X_S kg$_{COD}$ m^{-3}	X_{PG} kg$_{COD}$ m^{-3}	X_{EPS} kg$_{COD}$ m^{-3}	X_{EPSI} kg$_{COD}$ m^{-3}	X_I kg$_{COD}$ m^{-3}	S_S kg$_{COD}$ m^{-3}	S_I kg$_{COD}$ m^{-3}	$S_{I,PH}$ kg$_{COD}$ m^{-3}	S_{CO_2} kmol m^{-3}	S_{HCO_3} kmol m^{-3}	S_{NO_3} kmol m^{-3}	S_{NH_3} kmol m^{-3}	S_{O_2} kmol m^{-3}	
Phototrophs growth on CO$_2$ and nitrate	$\frac{32}{\phi+\varepsilon+1.3409}$				$\frac{32\phi}{\phi+\varepsilon+1.3409}$	$\frac{32\varepsilon}{\phi+\varepsilon+1.3409}$						$-\frac{\phi+\varepsilon+1.0025}{\phi+\varepsilon+1.3409}$		$-\frac{0.1704}{\phi+\varepsilon+1.3409}$		1	r1
Phototrophs growth on CO$_2$ and ammonia	$\frac{32}{\phi+\varepsilon+1}$				$\frac{32\phi}{\phi+\varepsilon+1}$	$\frac{32\varepsilon}{\phi+\varepsilon+1}$						$-\frac{\phi+\varepsilon+1.0025}{\phi+\varepsilon+1}$			$-\frac{0.1704}{\phi+\varepsilon+1}$	1	r2
Phototrophs growth on HCO$_3^-$ and nitrate	$\frac{32}{\phi+\varepsilon+1.3409}$				$\frac{32\phi}{\phi+\varepsilon+1.3409}$	$\frac{32\varepsilon}{\phi+\varepsilon+1.3409}$							$-\frac{\phi+\varepsilon+1.0025}{\phi+\varepsilon+1.3409}$	$-\frac{0.1704}{\phi+\varepsilon+1.3409}$		1	r3
Phototrophs growth on HCO$_3^-$ and ammonia	$\frac{32}{\phi+\varepsilon+1}$				$\frac{32\phi}{\phi+\varepsilon+1}$	$\frac{32\varepsilon}{\phi+\varepsilon+1}$							$-\frac{\phi+\varepsilon+1.0025}{\phi+\varepsilon+1}$		$-\frac{0.1704}{\phi+\varepsilon+1}$	1	r4
Phototrophs inactivation	-1			$1-f_{XI}-f_{SI,PH}$				f_{XI}			$f_{SI,PH}$				$\frac{0.0746-i_{N,XS}(1-f_{XI}-f_{SI,PH})-i_{N,XI}f_{XI}-i_{N,SI}f_{SI,PH}}{14}$		r5
Phototrophs respiration	$\frac{32 \cdot Y_{PH/PG}}{1-Y_{PH/PG}}$				$-\frac{32}{1-Y_{PH/PG}}$							$\frac{1-1.0025 \cdot Y_{PH/PG}}{1-Y_{PH/PG}}$			$-\frac{0.1704}{1-Y_{PH/PG}}$	-1	r6
Heterotrophs growth (aerob)			1						$-\frac{1}{Y_H}$			$\frac{1}{32 \cdot Y_H}-0.02976$			$-\frac{0.2}{33.6}$	$-\frac{1}{32 \cdot Y_H}+0.03125$	r7
Heterotrophs growth (anoxic)			1						$-\frac{1}{Y_H}$			$\frac{1}{32 \cdot Y_H}-0.02976$		$-\frac{0.8}{32 \cdot Y_H}+0.02857$			r8
Heterotrophs inactivation			-1	$1-f_{XI}$				f_{XI}							$\frac{0.083-i_{N,XS}(1-f_{XI})-i_{N,XI}f_{XI}}{14}$		r9
Nitrifiers growth		1										$-\frac{1}{33.6}$		$\frac{1}{14Y_N}$	$-\left(0.00593+\frac{1}{14Y_N}\right)$	$-\left(\frac{1}{7Y_N}-\frac{1}{32}\right)$	r10
Nitrifiers inactivation		-1		$1-f_{XI}$				f_{XI}							$\frac{0.083-i_{N,XS}(1-f_{XI})-i_{N,XI}f_{XI}}{14}$		r11
Hydrolysis				-1					$1-f_{SI}$	f_{SI}					$\frac{i_{N,XS}-i_{N,SI}f_{SI}}{14}$		r12
EPS hydrolysis						-1	$\frac{1}{1+\tau}$			$\frac{\tau}{1+\tau}$							r13

Table IV. Rate expressions of the biological processes in the PHOBIA model.

	Rates
r1	$q_{\max,O_2,PH} \cdot \min\left[\dfrac{S_{CO_2}}{K_{S,PH,CO_2}+S_{CO_2}}, \dfrac{S_{NO_3}}{K_{S,PH,NO_3}+S_{NO_3}}, \dfrac{K_{S,PH,NH_3}}{K_{S,PH,NH_3}+S_{NH_3}}, f_{I,PH}\right] \cdot X_{PH}$
r2	$q_{\max,O_2,PH} \cdot \min\left[\dfrac{S_{CO_2}}{K_{S,PH,CO_2}+S_{CO_2}}, \dfrac{S_{NH_3}}{K_{S,PH,NH_3}+S_{NH_3}}, f_{I,PH}\right] \cdot X_{PH}$
r3	$q_{\max,O_2,PH} \cdot \min\left[\dfrac{S_{HCO_3}}{K_{S,PH,HCO_3}+S_{HCO_3}}, \dfrac{S_{NO_3}}{K_{S,PH,NO_3}+S_{NO_3}}, \dfrac{K_{inh,PH,NH_3}}{K_{inh,PH,NH_3}+S_{NH_3}}, \dfrac{K_{inh,PH,CO_2}}{K_{inh,PH,CO_2}+S_{CO_2}}, f_{I,PH}\right] \cdot X_{PH}$
r4	$q_{\max,O_2,PH} \cdot \min\left[\dfrac{S_{HCO_3}}{K_{S,PH,HCO_3}+S_{HCO_3}}, \dfrac{K_{inh,PH,CO_2}}{K_{inh,PH,CO_2}+S_{CO_2}}, \dfrac{S_{NH_3}}{K_{inh,PH,NH_3}+S_{NH_3}}, f_{I,PH}\right] \cdot X_{PH}$
r5	$b_{ina,PH} \cdot X_{PH}$
r6	$0.1 \cdot q_{\max,O_2,PH} \cdot \min\left(\dfrac{S_{O_2}}{K_{S,PH,O_2}+S_{O_2}}, \dfrac{X_{PG}}{K_{S,PH,PG}+X_{PG}}, \dfrac{K_{inh,PH,I}}{K_{inh,PH,I}+I}\right) \cdot X_{PH}$
r7	$\mu_{\max,H} \cdot \min\left(\dfrac{S_{O_2}}{K_{S,H,O_2}+S_{O_2}}, \dfrac{S_S}{K_{S,H,SS}+S_S}, \dfrac{S_{NH_3}}{K_{S,H,NH_3}+S_{NH_3}}\right) \cdot X_H$
r8	$\mu_{\max,DN} \cdot \min\left(\dfrac{K_{S,H,O_2}}{K_{S,H,O_2}+S_{O_2}}, \dfrac{S_S}{K_{S,H,SS}+S_S}, \dfrac{S_{NO_3}}{K_{S,H,NO_3}+S_{NO_3}}\right) \cdot X_H$
r9	$b_{ina,H} \cdot X_H$
r10	$\mu_{\max,N} \cdot \min\left(\dfrac{S_{O_2}}{K_{S,N,O_2}+S_{O_2}}, \dfrac{S_{NH_3}}{K_{S,N,NH_3}+S_{NH_3}}, \dfrac{S_{CO_2}}{K_{S,N,CO_2}+S_{CO_2}}\right) \cdot X_N$
r11	$b_{ina,N} \cdot X_N$
r12	$k_h \cdot \dfrac{X_S/X_H}{K_{S,h,X}+X_S/X_H} \cdot X_H$
r13	$k_{h,EPS} \cdot \dfrac{K_{S,H,SS}}{K_{S,H,SS}+S_S} \cdot X_{EPS}$

The maximum specific O_2 consumption rate by phototrophs is $q_{\max,O_2,PH} = \dfrac{Y_{O_2/e^-} \cdot ETR_{max}}{\rho_{PH,ETR} \cdot L_{f,ETR} \cdot 0.9708}$, and the light dependency term is $f_{I,PH} = \dfrac{I/ETR_{max}}{\frac{I^2}{\alpha I_{opt}^2} + \left(\frac{1}{ETR_{max}} - \frac{2}{\alpha I_{opt}}\right)I + \frac{1}{\alpha}}$.

produced. For model simplification, both parameters are assumed to be constant in time. As information on yields of EPS and internally stored polyglucose is scarce, these parameters typically need to be determined via model fitting. The sensitivity of the model towards φ and ε is analyzed later in this paper.

The kinetics of photosynthetic growth in the PHOBIA model is based on the electron transfer rate (ETR), via the yield of oxygen produced per electron transferred, the maximum specific oxygen production rate is obtained. The phototrophic growth rate as well as the conversion rates of all the other compounds involved in phototrophic growth is derived from the oxygen production rate via yields obtained applying elemental balances.

Two independent processes of phototrophic growth in the light were implemented, which differ in their usage of nitrogen source. It has been shown that phototrophic microorganisms are able to utilize both ammonia-N and

nitrate-N for growth, whereby ammonia is the preferred N-source (Dortch, 1990). This was modeled via an inhibition term for ammonia in the nitrate-based phototrophic growth process. The specific rates of phototrophic growth on both ammonia and nitrate were assumed to be equal (Dortch, 1990).

It has been reported by various authors that phototrophs are able to utilize bicarbonate as their inorganic carbon source in situations where CO_2 is depleted (Goldman, 1999; Smith, 1983). This is of special importance in phototrophic biofilms, as in the inner layers of thick biofilms pH can become strongly alkaline due to diffusion limitations, thus resulting in a shift of the acid–base equilibrium towards bicarbonate. The PHOBIA model therefore distinguishes between different phototrophic growth reactions using CO_2 and bicarbonate as carbon source, respectively, whereby HCO_3^--based growth is inhibited by the presence of CO_2.

Table V. Stoichiometry and kineticsof chemical reactions.

Process	Solubles					Rate
	S_{NH_3} kmol m^{-3}	S_{NH_4} kmol m^{-3}	S_{CO_2} kmol m^{-3}	S_{HCO_3} kmol m^{-3}	S_{CO_3} kmol m^{-3}	
Dissociation HCO_3^-				-1	1	$k_{AB,HCO_3/CO_3} \cdot (S_{HCO_3} - S_H \cdot S_{CO_3}/K_{a,HCO_3/CO_3})$
Hydration CO_2 (H_2O)			-1	1		$k_{AB,CO_2/H_2O} \cdot (S_{CO_2} - S_{HCO_3} \cdot S_H/K_{a,CO_2/H_2O})$
Hydration CO_2 (OH)			-1	1		$k_{AB,CO_2/OH} \cdot (S_{CO_2} \cdot K_{a,H_2O}/S_H - S_{HCO_3}/K_{a,CO_2/OH})$
Dissociation NH_3	1	-1				$k_{AB,NH_3/NH_4} \cdot (S_{NH_4} - S_H \cdot S_{NH_3}/K_{a,NH_3/NH_4})$

The light dependency of phototrophic growth was modeled via the Eilers–Peeters relationship (Eilers and Peeters, 1988), which accounts for light saturation and photoinhibition at high irradiances. It relies on three parameters to describe the photosynthetic production rate as a function of light intensity: The maximum (optimum) rate ETR_{max}, the initial slope α of the ETR(I) curve, and the light intensity I_{opt} corresponding to ETR_{max}, see Figure 2. Using this approach, the term $f_{I,PH}$ that describes the light limitation of the photosynthetic growth kinetics (cf. also Equations (1) and (2)) is obtained in Equations (3) and (4):

$$f_{I,PH}(I) = \frac{I/ETR_{max}}{aI^2 + bI + c} \tag{3}$$

with

$$a = \frac{1}{\alpha I_{opt}^2}, \quad b = \frac{1}{ETR_{max}} - \frac{2}{\alpha I_{opt}}, \quad c = \frac{1}{\alpha} \tag{4}$$

The PHOBIA model also takes photoadaptation into account. According to (Zonneveld, 1998), photoadaptation is a phenomenon by which the phototrophic cell responds to changes in irradiance on a long time-scale (in the order of several hours or days). This response is expressed by alterations in cellular pigment (chlorophyll) contents and cell morphology. Generally, intracellular chlorophyll contents are higher under dark conditions than when exposed to light.

In this model, the approach of Duarte and Ferreira (1997) was followed, who incorporated photoadaptation into the Eilers and Peeters model (Eqs. 3 and 4). It is assumed that photoadaptation causes dynamics in the initial slope α of the ETR(I) curve. This dynamics is modeled via the introduction of the chlorophyll/carbon ratio (Eq. 5):

$$\alpha = \frac{ETR_{max}}{I_n(0.25 - 5R)} \tag{5}$$

where I_n is the maximum incident irradiance ("irradiance at noon") and R is the chlorophyll to carbon ratio. Duarte

and Ferreira implemented the chlorophyll/carbon ratio as a dynamic state variable r_R,

$$r_R = \frac{dR}{dt} = \gamma(R_w - R) \tag{6}$$

based on a model presented earlier by Falkowski and Wirick (1981). γ is a kinetic coefficient that equals $0.2\ h^{-1}$ during periods of light and 0 during periods of darkness. R_w is the chlorophyll/carbon ratio towards which the cells adapt, which is calculated as Equation (7):

$$R_w = \begin{cases} 0.04 & I/I_n < 0.01 \\ 0.01 + 0.03\frac{\ln(I/I_n)}{\ln(0.01)} & I/I_n \geq 0.01 \end{cases} \tag{7}$$

Light attenuation across the biofilm was modeled by the Lambert-Beer law (Eq. 8):

$$I(t,z) = I_{in}(t) \cdot e^{-k_{tot}(L_f - z)\sum_i X_i} \tag{8}$$

where I_{in} is the incident light intensity on top of the biofilm and z the biofilm space coordinate perpendicular to the biofilm surface, measured from substratum. X_i is the concentration of the particulate compounds i in the biofilm. The light attenuation coefficient k_{tot} across the whole biofilm can be determined experimentally according to Equation (9):

$$k_{tot} = -\frac{\ln(I_{out}/I_{in})}{\rho_b \cdot L_f} \tag{9}$$

where I_{out} is the light intensity measured across the biofilm, ρ_b is the overall biofilm density and L_f is the biofilm thickness in the experimental conditions.

Dynamics in incident light intensity, such as light–dark cycles, are implemented via the variable I_{in}, which in that case becomes a function of light intensity, dependent on time. In the simulations presented later in this paper, both on–off switching functions and continuous functions are applied. Their respective use is mentioned where appropriate.

Photorespiration, that is, oxygen consumption during light exposure due to the oxygenase function of RubisCO, occurring preferentially under high temperatures and high oxygen concentrations, is not explicitly modeled in the PHOBIA model. Rather, it is implicitly incorporated in the phototrophic growth rate via the yield coefficient of oxygen on transferred electrons.

Photoautotrophic Growth: Dark Respiration

In the absence of light, organic matter and oxygen are consumed by the phototrophs, and carbon dioxide as well as new biomass are produced (Kromkamp, 1987). This process is termed dark respiration in the following sections. It is assumed
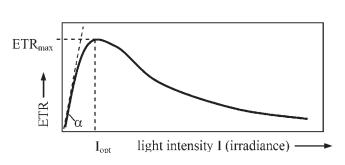

Figure 2. Illustration of the three parameters determining the ETR(I)-curve in the Eilers and Peeters model: The maximum (optimum) rate ETR_{max}, the initial slope α of the ETR(I) curve, and the light intensity I_{opt} corresponding to ETR_{max}.

that the organic matter utilized stems from the intracellular polyglucose pool, which was built up in the light-driven processes (Kromkamp, 1987; Smith, 1983; Thorud and Sirevag, 1982). Phototrophic respiration in the absence of light is typically assumed to be about 10% of the maximum oxygen production rate in the light (Tillmann and Rick, 2001).

Chemical Conversion Processes

Acid–base equilibria were included in the PHOBIA model, as a pre-requisite for calculating pH profiles and for determining the availability of inorganic carbon for autotrophic growth. Ionic speciation was modeled from mass action laws and charge balance. The ionic species considered comprise soluble inorganic carbonaceous as well as ammonacious compounds. An overview of the modeled acid–base reactions as well as the associated dissociation constants, rate constants, and rates is presented in the Tables I and V.

The concentration of protons was calculated from charge balance, for example:

$$S_H + S_{NH_4} + S_{cat} - S_{HCO_3} - S_{NO_3} - 2S_{CO_3} - S_{OH} - S_{an} = 0 \quad (10)$$

where by

$$(S_{cat} + S_{NH_4} - S_{an} - S_{HCO_3} - S_{NO_3} - 2S_{CO_3}) = \sum_i (S_{i,ion}) \quad (11)$$

and

$$S_{OH} = \frac{K_{a,H_2O}}{S_H} \quad (12)$$

Substituting Equations (11) and (12) into Equation (10) and re-arranging yields Equation (13) for the calculation of S_H, where pH (14) can be determined from

$$S_H = 0.5 \left(\sqrt{\left(\sum_i (S_{i,ion}) \right)^2 + 4K_{a,H_2O}} - \sum_i (S_{i,ion}) \right) \quad (13)$$

$$pH = -\log(S_H) \quad (14)$$

Biofilm Detachment

The biofilm detachment rate, r_d, was implemented as a continuous empirical function, dependent on the ratio of the current biofilm thickness L_f and a maximum imposed biofilm thickness $L_{f,max}$. For small biofilm thickness, the detachment rate approximates zero and at maximum biofilm thickness it equals the biofilm front velocity, u_F:

$$r_d = u_f \left(\frac{L_f}{L_{f,max}} \right)^{n_d} \quad (15)$$

The steepness of the switching function (15) can be adjusted by varying the exponent n_d. The value $n_d = 10$ was used in the simulations presented herein.

Results and Discussion

A number of processes included in the PHOBIA model have extensively been studied in the past, such as nitrification, aerobic, and anoxic heterotrophic growth. Typical kinetic parameters for those processes are widely documented in the literature and are part of well-established aquatic models, such as the Activated Sludge Model (Henze et al., 2000) or the River Water Quality Model (Reichert, 2001). For other processes, experimental observations are still scarce. This is the case for the EPS formation and internal polyglucose storage in phototrophs. Determining EPS production in mixed phototrophic biofilms is especially problematic, as part of the excreted organic compounds is simultaneously consumed by heterotrophs. The values of the stoichiometric parameters ε (relative rate of EPS formation to phototrophic biomass production) and ϕ (relative rate of formation of internally stored polyglucose to phototrophic biomass production) in the PHOBIA model relating to these two phenomena therefore presently need to be assumed or obtained by model fitting. Therefore, it is advantageous to have information on the influence of these parameters on the overall model.

The sensitivity of model predictions was analyzed for four different values of ε, ranging from 0.1 to 0.4 g COD (EPS)/g COD (phototrophic biomass PH) (maintaining ϕ at 0.1 g COD/g COD). With regard to ϕ, Dircks et al. (2001) found stored glycogen fractions between 0.05 and 0.18 g COD (glucose)/g COD (biomass) under aerobic conditions in mixed cultures subjected to feast-famine regimes, and Merrick (1978) reported internally stored glucose fractions of 0.07 g COD (glucose)/g COD (biomass) for the phototrophic species *Chromatium vinosum*. These values were achieved in the model applying ϕ-values between 0.1 and 0.4 g COD (PG)/g COD (PH) (keeping ε constant at 0.3 g COD (EPS)/g COD (PH)), which consequently was the range of ϕ chosen for sensitivity analysis.

Simulations were carried out for a 15 days period of phototrophic biofilm development, until a pseudo-steady-state was reached. On–off light cycles of 8 h darkness and 16 h light were applied in the simulations with a constant incident light intensity of 120 μmol photons/m^2/s in the light period. The remaining model parameters are listed in the Table VI.

The following sections give a short overview on general observations from the model simulations, followed by a sensitivity analysis of ε and ϕ.

General Observations

Phototrophic biofilm development during the simulated 15 days period exhibited an initial lag phase of about 3 days, followed by an exponential growth phase. After approximately 13 days a pseudo-steady state "mature" phase was reached, which was dictated by biofilm detachment kinetics, that is, biofilm growth and detachment were in equilibrium. This is in accordance with experimental observations within the PHOBIA project. During light periods, an increase in biofilm thickness was observed, while in the darkness a slight decrease was apparent. The reasons for this are further expanded on below. At high biofilm thickness, phototrophic growth kinetics was found to be considerably influenced by light attenuation as well as pH and carbon substrate gradients across the biofilm. Near the biofilm substratum, pH values above 10 were predicted during the light periods, as compared to a pH of 7.5 at the biofilm surface. Furthermore, enhanced oxygen levels were predicted near the biofilm base in the presence of light, amounting to about three times the values at the biofilm surface. A detailed analysis and discussion of these phenomena and their comparison with experimental findings is the subject of a forthcoming paper.

Relative Rate of EPS Formation to Phototrophic Biomass Production

The influence of EPS production on biofilm thickness evolution is illustrated in Figure 3a. During light periods, an increase in biofilm thickness is observed, predominantly due to phototrophic growth and associated EPS formation. During darkness, these processes cease and only phototrophic dark respiration contributes to biofilm growth, though at a lower growth rate. The EPS formed during the light periods is continuously hydrolyzed and consumed by heterotrophic biomass, irrespective of the light conditions. Therefore, during dark periods the consumption of EPS leads to a volume loss and to net decrease in biofilm thickness. The higher the ε-values, the less phototrophic biomass is produced relative to EPS. Therefore, higher ε results in smaller phototrophic growth rates due to the lower concentrations of X_{PH} (see Fig. 3b), and consequently the increase of biofilm thickness during the light periods in Figure 3a is slower, especially in the exponential growth phase.

Interesting is also the evolution of heterotrophic biomass as a function of ε, as illustrated in Figure 3c. The initial biofilm composition was assumed to contain equal fractions of phototrophs, heterotrophs, and nitrifiers. During the initial biofilm growth phase a sharp decrease in hetero-

trophic biomass is observed. This is due to limitation by readily available organic carbon, which is not supplied externally to the system, but needs to be produced internally via EPS and biomass death and lysis. Once sufficient organic carbon is supplied internally by EPS production and hydrolysis, a continuous increase in heterotrophic biomass is observed. One would assume to observe higher heterotrophic concentrations at higher ε, as more organic substrate in the form of EPS is produced. This can be indeed noted during the exponential biofilm growth phase from about Day 5 to 10. Still, this effect is less pronounced as might be expected from the difference in organic carbon availability at different values of ε, because heterotrophic growth is not only limited by EPS production, but also by EPS hydrolysis to a large extent. However, towards the end of the exponential biofilm growth phase, slightly higher heterotrophic growth is observed at lower EPS production rates, which can be explained as follows. While in thin biofilms heterotrophic activity is fueled by EPS produced across the whole biofilm thickness, in thick biofilms the inner layers become photosynthetically inactive due to diffusion limitations and light extinction. EPS is generated only in the active upper biofilm layer in relatively constant amounts. On the other hand, increasing inactivation of phototrophic biomass takes place in the inner biofilm layers, and more organic carbon is supplied to the heterotrophs via biomass lysis. Consequently, the biofilm which contains more (decaying) phototrophic biomass, that is, the one with lower ε, has a higher apparent heterotrophic growth rate, and hence a higher X_H. In addition, in the model the carbon supply rate from hydrolysis of dead biomass is higher than that from EPS. While the EPS hydrolysis rate constant was taken from a study on heterotrophic biofilms (Horn et al., 2001), in mixed phototrophic biofilms different kinetics may prevail, due to different EPS composition. More in-depth studies on EPS production by phototrophs, and on EPS composition and hydrolysis are desirable for a more realistic estimation of $k_{h,EPS}$.

In Figure 4 profiles of pH (Fig. 4a) and dissolved oxygen (Fig. 4b) across the biofilm are depicted for different values of ε for a biofilm of 500 μm thickness. The simulated values are in the same order of magnitude as experimentally observed values within the PHOBIA project (Staal et al., 2007). At the base of the phototrophic biofilm a large increase in pH is observed during the light periods, which is caused by the depletion of CO_2 and bicarbonate buffer, due to diffusion limitation as well as consumption by autotrophic biomass. Furthermore, oxygen production by phototrophic biomass in the light leads to increased oxygen levels near the biofilm base.

There is a distinct influence of ε on both pH and S_{O_2}, with pH differing by about 0.7 and S_{O_2} by 0.25 mM (about 40% in relative terms) at the biofilm base for ε-values between 0.1 and 0.4. This is mainly owing to the different concentrations of phototrophs in the biofilms. When more phototrophic biomass is present, that is, at low ε values, more oxygen is produced and more CO_2 and bicarbonate are consumed,

Table VI. Overview of model parameters.

Model parameter	Symbol	Value	Unit	Reference
Kinetic parameters				
Maximum electron transfer rate at 120 $\mu mol\ m^{-2}\ s^{-1}$ incident intensity	$ETR_{max,120}$	2.246×10^{-3}	$kmol(e^-)\ m^{-2}\ d^{-1}$	PHOBIA experiments
Optimum intensity at 120 $\mu;mol\ m^{-2}\ s^{-1}$ incident intensity	$I_{opt,120}$	1.814×10^{-2}	$kmol(phot)\ m^{-2}\ d^{-1}$	PHOBIA experiments
Light extinction coefficient	k_{tot}	210	$m^2\ kg^{-1}$	PHOBIA experiments
Initial chlorophyll/carbon ratio	R_0	0.04		Duarte and Ferreira (1997)
Rate coefficient of chlorophyll/carbon ratio	γ	4.8 (during light) 0 (during darkness)	d^{-1}	Duarte and Ferreira (1997)
Maximum specific growth rate nitrifiers	$\mu_{max,N}$	1	d^{-1}	Henze et al. (2000)
Maximum aerobic specific growth rate heterotrophs	$\mu_{max,H}$	5.5	d^{-1}	Horn and Hempel (1997)
Maximum anoxic specific growth rate heterotrophs (denitrification)	$\mu_{max,DN}$	1.6	d^{-1}	Reichert et al. (2001)
Inactivation rate constant for phototrophs	$b_{ina,PH}$	0.09	d^{-1}	[a]
Inactivation rate constant for chemoautotrophs	$b_{ina,N}$	0.15	d^{-1}	Henze et al. (2000)
Inactivation rate constant for heterotrophs	$b_{ina,H}$	0.4	d^{-1}	Henze et al. (2000)
CO_2 half saturation coefficient phototrophs	K_{S,PH,CO_2}	10^{-4}	$kmol(CO_2)\ m^{-3}$	Goldman (1999)
NO_3^- half saturation coefficient phototrophs	K_{S,PH,NO_3}	1.2×10^{-6}	$kmol(NO_3)\ m^{-3}$	Eppley et al. (1969)
NH_3 half saturation coefficient phototrophs	K_{S,PH,NH_3}	1.2×10^{-6}	$kmol(NH_3)\ m^{-3}$	Eppley et al. (1969)
O_2 half saturation coefficient phototrophs	K_{S,PH,O_2}	3×10^{-4}	$kmol(O_2)\ m^{-3}$	[b]
Light inhibition coefficient for phototrophs (dark respiration)	$K_{inh,PH,I}$	8×10^{-5}	$kmol(e^-)\ m^{-2}\ d^{-1}$	[c]
CO_2 inhibition coefficient for phototrophic growth on HCO_3^-	K_{inh,PH,CO_2}	10^{-6}	$kmol(CO_2)\ m^{-3}$	[c]
NH_3 inhibition coefficient for phototrophic growth on nitrate	K_{inh,PH,NH_3}	1.2×10^{-6}	$kmol(NH_3)\ m^{-3}$	Assumed the same as K_{S,PH,NH_3}
Half saturation coefficient for internal polyglucose usage	$K_{S,PH,PG}$	0.005	$kg\ COD\ m^{-3}$	Smith (1983)
CO_2 half saturation coefficient nitrifiers	K_{S,N,CO_2}	10^{-4}	$kmol(CO_2)\ m^{-3}$	[d]
NH_3 half saturation coefficient nitrifiers	K_{S,N,NH_3}	7.14×10^{-5}	$kmol(NH_3)\ m^{-3}$	Henze et al. (2000)
O_2 half saturation coefficient nitrifiers	K_{S,N,O_2}	1.56×10^{-5}	$kmol(O_2)\ m^{-3}$	Henze et al. (2000)
Readily degradable organic substrate half saturation coefficient heterotrophs	$K_{S,H,SS}$	0.004	$kg(COD)\ m^{-3}$	Henze et al. (2000)
Particulate COD half saturation coefficient	$K_{S,h,X}$	0.1	$kg\ COD/kg\ COD$	Henze et al. (2000)
NH_3 half saturation coefficient heterotrophs	K_{S,H,NH_3}	10^{-10}	$kmol(NH_3)\ m^{-3}$	[e]
NO_3 half saturation coefficient denitrifiers	K_{S,H,NO_3}	3.6×10^{-5}	$kmol(NO_3)\ m^{-3}$	Reichert et al. (2001)
O_2 half saturation coefficient heterotrophs	K_{S,H,O_2}	6.25	$kmol(O_2)\ m^{-3}$	Henze et al. (2000)
X_s-hydrolysis rate constant	k_h	3	d^{-1}	Henze et al. (2000)
EPS-hydrolysis rate constant	$k_{h,EPS}$	0.34	d^{-1}	Horn et al. (2001)
Rate constant CO_2 hydrolysis	$k_{AB,CO_2/H_2O}$	2,221	d^{-1}	Ebrahimi et al. (2003)
Rate constant CO_2 hydrolysis at high pH	$k_{AB,CO_2/OH}$	7.19×10^8	d^{-1}	Ebrahimi et al. (2003)

(*Continued*)

Table VI. (*Continued*)

Model parameter	Symbol	Value	Unit	Reference
Rate constant HCO_3^--protolysis	$k_{AB,HCO_3/CO_3}$	10^{12}	d^{-1}	Assumed (fast equilibrium)
Rate constant ammonia dissociation	$k_{AB,NH_3/NH_4}$	10^{12}	d^{-1}	Assumed (fast equilibrium)
Dissociation constant CO_2 hydrolysis	$pK_{a,CO_2/H_2O}$	6.36		Ebrahimi et al. (2003)
Dissociation constant CO_2 hydrolysis at high pH	$pK_{a,CO_2/OH}$	-7.64		Ebrahimi et al. (2003)
Dissociation constant HCO_3^--protolysis	$pK_{a,HCO_3/CO_3}$	10.33		Ebrahimi et al. (2003)
Dissociation constant autoprotolysis of water	pK_{a,H_2O}	14		Ebrahimi et al. (2003)
Dissociation constant ammonia dissociation	pK_{a,NH_3}	9.680		Musvoto et al. (2000)
Stoichiometric parameters				
Yield of oxygen produced per electron transferred	$Y_{O_2/e-}$	0.160	kmol (O_2) kmol $(e-)^{-1}$	Morris and Kromkamp (2003)
Relative rate of EPS formation to phototrophic biomass production	ε	0.1–0.4	kg COD(EPS)/kg COD(PH)	Sensitivity analysis
Relative rate of formation of internally stored polyglucose to phototrophic biomass production	ϕ	0.1–0.4	kg COD(PG)/kg COD(PH)	Sensitivity analysis
Yield of nitrifiers on NO_3^-	Y_N	0.240	kg COD(X_N)/kg NO_3-N	Henze et al. (2000)
Yield of heterotrophs on S_S	Y_H	0.630	kg COD(X_H)/kg COD	Henze et al. (2000)
Ratio soluble to inert EPS production	τ	4	kg COD(S_S)/kg COD(X_{EPSI})	PHOBIA experiments fitting
Fraction of particulate inert COD in biomass	f_{XI}	0.100	kg COD(X_I)/kg COD (X_H, X_N, X_{PH})	Henze et al. (2000)
Fraction of soluble inert COD in particulate substrate	f_{SI}	0.190	kg COD(S_I)/kg COD(X_S)	Assumed
Fraction of soluble inert COD in phototrophic biomass	$f_{SI,PH}$	0.001	kg COD(S_I)/kg COD(X_{PH})	Assumed
Fraction of N in slowly degradable particulate organic matter	$i_{N,XS}$	0.043	kg N/kg COD (X_S)	Assumed
Fraction of N in particulate inert organic matter	$i_{N,XI}$	0.040	kg N/kg COD (X_I)	Assumed
Fraction of N in soluble inert organic matter	$i_{N,SI}$	0.010	kg N/kg COD (S_I) or kg N/kg COD ($S_{I,PH}$)	Assumed Henze et al. (2000)
Transport parameters				
Diffusion coefficient of CO_2 in water	D_{CO_2}	1.65×10^{-4}	$m^2\ d^{-1}$	Ebrahimi et al. (2003)
Diffusion coefficient of HCO_3^- in water	D_{HCO_3}	1.02×10^{-4}	$m^2\ d^{-1}$	Ebrahimi et al. (2003)
Diffusion coefficient of CO_3^{2-} in water	D_{CO_3}	7.9×10^{-5}	$m^2\ d^{-1}$	Ebrahimi et al. (2003)
Diffusion coefficient of O_2 in water	D_{O_2}	1.73×10^{-4}	$m^2\ d^{-1}$	Picioreanu et al. (1997)
Diffusion coefficient of NO_3^- in water	D_{NO_3}	1.47×10^{-4}	$m^2\ d^{-1}$	Picioreanu et al. (1997)
Diffusion coefficient of cations in water (assumed as Na^+)	D_{cat}	1.15×10^{-4}	$m^2\ d^{-1}$	Ebrahimi et al. (2003)
Diffusion coefficient of H^+ in water	D_{H+}	10^{-20}	$m^2\ d^{-1}$	f
Biofilm parameters				
Density of phototrophic biofilm	ρ_b	170	kg COD m^{-3}	PHOBIA experiments
Density of phototrophic biomass for ETR determination	$\rho_{PH,ETR}$	50	kg PH m^{-3}	PHOBIA experiments
Density of EPS	ρ_{EPS}	$\rho_b/6$	kg COD m^{-3}	Horn et al. (2001)

(*Continued*)

Table VI. (*Continued*)

Model parameter	Symbol	Value	Unit	Reference
Density of internal polyglucose	ρ_{PG}	$\rho_b \times 20$	kg COD m^{-3}	Assumed as very dense
Initial biofilm thickness	$L_{f,ini}$	1×10^{-5}	m	Assumed
Maximum biofilm thickness	$L_{f,max}$	10^{-3}	m	Defined
Thickness of biofilm used for ETR determination	$L_{f,ETR}$	10^{-4}	m	PHOBIA experiments
Total biofilm area	A_b	0.15	m^2	Approximated from PHOBIA incubator
Initial fraction of phototrophs in biofilm	ν_{PH}	0.1	kg COD/kg COD	[g]
Initial fraction of heterotrophs in biofilm	ν_H	0.1	kg COD/kg COD	[g]
Initial fraction of nitrifiers in biofilm	ν_N	0.1	kg COD/kg COD	[g]
Operational and reactor parameters				
Liquid bulk volume	V_{bulk}	3×10^{-3}	m^3	[h]
Incident light intensity	$I_{in,120}$	1.0368×10^{-2}	kmol(phot) m^{-2} d^{-1}	[h]
Inlet flow rate (medium)	Q_{in}	1	m^3 d^{-1}	[h]
Inlet concentration of HCO$_3^-$	$S_{HCO_3,in}$	1.5×10^{-3}	kmol(HCO$_3$) m^{-3}	[h]
Inlet concentration of O$_2$	$C_{O_2,in}$	2.8×10^{-4}	kmol(O$_2$) m^{-3}	[h]
Inlet concentration of NO$_3$-N	$S_{NH_4,in}$	10^{-3}	kmol m^{-3}	[h]
pH setpoint in bulk medium	pH$_{setpoint}$	7.5		[h]

[a]Assumed about 1/10 of maximum phototrophic growth rate.
[b]Assumed the same as for nitrifiers in Wiesmann (1994).
[c]Assumed value to assure switch-function.
[d]Assumed the same as for phototrophs.
[e]Very small limitation assumed, but nevertheless needed in order not to obtain negative NH$_3$ concentrations due to unlimited consumption.
[f]Protons were assumed in the numerical scheme used here as non-diffusive because their concentration is computed from the association with other diffusible ions (charge balance, Equation [13]).
[g]Initial fractions of biomass assumed so that the total is 0.3. The biofilm model in AQUASIM assumes a biofilm phase made of two sub-phases: Biofilm matrix (here with a volume fraction 0.3) and pore water (the rest 0.7).
[h]From PHOBIA experiments all operational and reactor parameters.

resulting in higher pH levels inside the biofilm due to a reduced buffering capacity.

Relative Rate of Internal Polyglucose to Phototrophic Biomass Formation

The influence of the relative rate of internal polyglucose to phototrophic biomass formation ϕ on biofilm thickness is less pronounced than with varying ε. This is because the difference in phototrophic biomass concentration between the four values of ϕ is small, amounting to a maximum of only 1.8 kg COD/m^3 biofilm, considering the daily average of X_{PH}. High values of ϕ mean that in the light more internal reserves are stored, which are available in the subsequent dark periods as carbon source for phototrophic growth via the dark respiration metabolism. Thus, the more internal glucose is stored during the light, the higher the phototrophic growth rate in the dark and the less decrease in biofilm thickness in darkness are observed. Besides counteracting biofilm volume loss due to EPS consumption by heterotrophs, phototrophic growth in the darkness also balances differences in X_{PH} from the previous light phase (where higher ϕ means that less carbon is channeled into X_{PH}), so that on a daily average base the difference in X_{PH} is

minimal for varying values of ϕ. Consequently, the impact of ϕ on pH and oxygen profiles during light periods becomes negligible, as inorganic carbon consumption and oxygen production are largely determined by X_{PH}.

In conclusion, it can be said that it is generally desirable to obtain more experimentally based information on both EPS production and internal storage kinetics. For the PHOBIA model as such, the correctness of the EPS kinetics is more important than that of internal glucose storage, as it exhibits a higher sensitivity to ε than to ϕ.

Potential of Phototrophic Biofilms for Wastewater Treatment

In order to assess the potential of using phototrophic biofilms for wastewater polishing, it is useful to compare them to planktonic systems that are commonly applied for this purpose. In what follows, the potential N uptake rate of a model phototrophic biofilm is analyzed and compared with that of an algal pond for wastewater stabilization.

A simulation was carried out where a phototrophic biofilm was subjected to dynamic light–dark cycles of 24 h duration with a maximum incident light intensity of 1,500 µmol photons m^{-2} s^{-1}, similar to those observed in
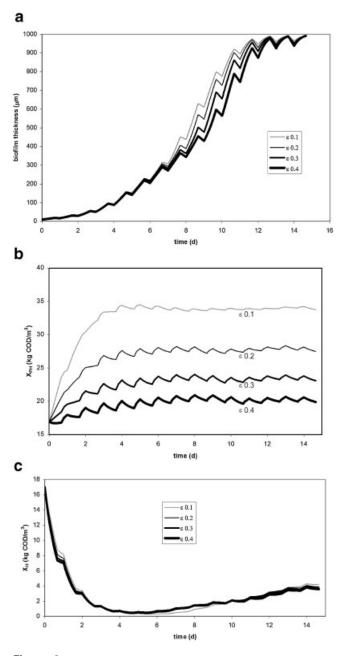
Figure 3. Evolution of **a**: biofilm thickness and concentration of **b**: phototrophic, and **c**: heterotrophic biomass for four different values of ε between 0.1 and 0.4.

Figure 4. Profiles of **a**: pH and **b**: oxygen concentration across the biofilm at 500 μm biofilm thickness (exponential growth stage) for four different values of ε between 0.1 and 0.4 kg COD (EPS)/kg COD(X_{PH}).

nature. The dynamic incident light function was implemented as described by Pahl-Wostl (1992).

Figure 5 depicts the evolution of the average net N accumulation rate during the light in a phototrophic biofilm grown over a period of 50 days. This is compared with average N removal rates from an algal pond for wastewater stabilization documented by Zimmo et al. (2004), whereby only biological N removal was taken into consideration. Figure 5 shows that from a biofilm thickness of about 630 μm the average net N uptake rate of the phototrophic
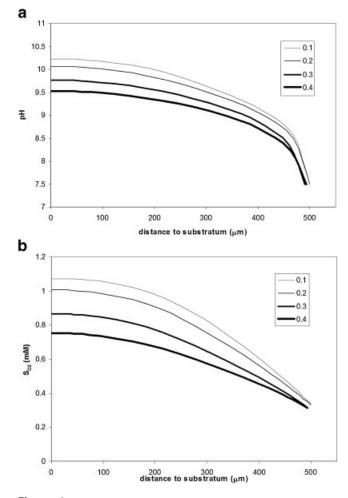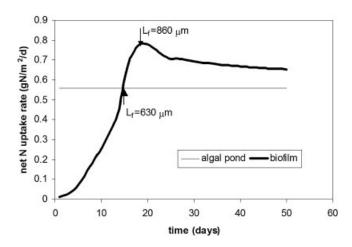

Figure 5. Cumulative areal N-uptake rates of phototrophic biofilm and conventional algal pond.

biofilm exceeds that of the conventional algal pond, being about 1.4 times as high at an optimum biofilm thickness of about 860 μm. This confirms the assumption that phototrophic biofilms can considerably enhance nutrient uptake rates in tertiary wastewater treatment. It is likely that the real N accumulation rates of biofilms grown at natural light even exceed those presented here, as the simulations are based on photosynthetic production rates of a biofilm adapted to a much lower light intensity (120 μmol photons m^2 s^{-1}). Maximum photosynthetic production in a daylight-adapted biofilm is likely to be higher, resulting in higher growth rates and consequently higher N-uptake rates.

In the simulated case, the vast majority of N-removal occurred due to N-incorporation into phototrophic biomass rather than nitrification (see Fig. 6). Nitrifiers growth was insignificant and turned out to be limited mainly by the availability of CO_2 due to competition with phototrophic biomass. This phenomenon is analyzed in more detail in a forthcoming paper on the PHOBIA case study.

Conclusions

This paper presents a first approach in the mathematical modeling of the dynamics of phototrophic biofilms. The PHOBIA model specifically focuses on interactions between different functional groups of microorganisms. Emphasis was put on including a number of key mechanisms specific to phototrophic biofilm communities, which to our knowledge have not been modeled before in this context, such as EPS production and internal polyglucose storage by phototrophs, ability of phototrophs to utilize bicarbonate in the absence of CO_2, and explicit distinction between ammonia and nitrate as N-source. This model can serve as a base for further experimental work, as it indicates which parameters are sensitive and therefore need more analysis.
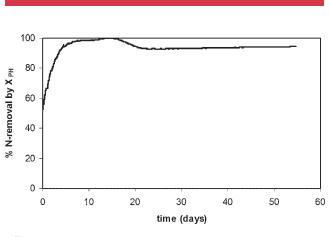

Figure 6. Contribution of phototrophic biomass to overall N-removal rate.

Appendix—Definition of PHOBIA-Model Specific State Variables

X_{PH} (kg$_{COD}$ m^{-3}): Photoautotrophic Biomass

This component stands for the group of microorganisms that is able to utilize light as energy source and inorganic carbon as substrate. The group of phototrophic microorganisms comprises a vast range of genera and microbial species, amongst them are green algae, cyanobacteria (also termed green–blue algae) and diatoms. However, as this model focuses on the interaction between different functional groups of microorganisms rather than different species, it was opted for not making any further subdivision of "phototrophs." This is further supported by experimental evidence, which showed that in phototrophic biofilms grown under identical conditions in different laboratories the composition of phototrophic species varied strongly, although reproducibility at the functional and developmental level was high (Roeselers et al., 2006). This warrants the assumption that the behavior of phototrophic biofilm systems is governed by differences at the functional rather than at phototrophic species level.

The lump group of photoautotrophic organisms is therefore assumed to exhibit a set of common generic properties with regard to the kinetics of substrate and nutrient usage, which distinguish it from the other two principal metabolic groups in the model, that is, chemoautotrophs and heterotrophs. Furthermore, it was supposed that photoautotrophic biomass has two distinct mechanisms for handling carbon not used for biomass synthesis, that is, external excretion and intracellular storage. The elemental compositions of phototrophic biomass was taken as $CH_{2.5}ON_{0.17}$ (Falkowski et al., 1985), whereas heterotrophic and chemoautotrophic biomass was assumed as $CH_{1.8}O_{0.5}N_{0.2}$.

X_{EPS} (kg$_{COD}$ m^{-3}): Extracellular Polysaccharides and Exudates

In the presence of surplus carbon and energy, phototrophic microorganisms may excrete large amounts of polysaccharides into the surrounding medium (Smith and Underwood, 2000; Stal, 2003). EPS formation is of key importance especially in biofilm development, as it creates an adhesive matrix promoting biomass attachment and aggregation. Furthermore, if hydrolyzed, part of the excreted EPS may serve as organic carbon source enabling heterotrophic growth in the biofilm. In this model, X_{EPS} denotes the sum of extracellular polysaccharides excreted by photoautotrophs. Usually, little is known about the actual composition of the complex mixtures of excreted organic substances and about detailed kinetics of EPS formation. For the stoichiometry of processes involved in this model, exudates and EPS were modeled as having the elemental formula of polyglucose (CH_2O).

X_{EPSI} (kg_{COD} m^{-3}): Inert EPS

This component represents the inert fraction of the excreted EPS, which is not available as organic carbon source for heterotrophic biomass upon EPS hydrolysis.

X_{PG} (kg_{COD} m^{-3}): Internally Stored Polyglucose

Another pathway followed by some microorganisms in the presence of surplus carbon and energy is the intracellular storage of polymers. This mechanism serves to build internal reserves of carbon and energy, which can be later utilized in periods of substrate limitation. Often, accumulation of internal reserves in microorganisms is enhanced as response to alternating feast-famine regimes (van Loosdrecht et al., 1997). For phototrophs, intracellular storage of polymers (represented generically here for stoichiometry reasons as polyglucose) was shown to be promoted under alternating light–dark conditions (Kromkamp, 1987; Sirevag and Ormerod, 1977; Smith, 1983).

$S_{I,PH}$ (kg COD m^{-3}): Inert Soluble COD From Inactivation of Phototrophis Biomass

This arbitrary non-reactive and non-diffusive compound is introduced in the inactivation reaction of phototrophic biomass. Its introduction is needed for elemental balancing, as the phototrophic biomass has a different elemental composition than the heterotrophic and chemoautotrophic biomass groups, and it is assumed that during inactivation all three biomass groups form the same products X_S ($CH_{1.5}O_{0.5}N_{0.1}$) and X_I ($CH_{1.58}O_{0.5}N_{0.098}$).

S_{CO2}, S_{HCO_3}, and S_{CO_3} (kmol m^{-3}): Carbon Dioxide, Bicarbonate, and Carbonate

The model takes three different inorganic carbon (IC) species into account, that is, carbon dioxide, as well as the bicarbonate and carbonate anions. Both CO_2 and HCO_3^- are used as carbon and energy source by phototrophs and nitrifiers (Goldman, 1999; Kirk, 1994). The two ionic species HCO_3^- and CO_3^{2-} arise from the hydration of CO_2 and the associated acid–base equilibria, which are a function of the local pH. At pH values below six, CO_2 is the dominant IC-species, between about 6 and 10 the equilibrium shifts to the bicarbonate ion, whereas at pH above 10 the carbonate ion becomes dominant.

S_{NH_3}, S_{NH_4}, and S_{NO_3} (kmol m^{-3}): Ammonia, Ammonium, and Nitrate Nitrogen

Three dissolved nitrogen compounds are included in the model, that is, ammonia, the ammonium ion, and the nitrate ion. Ammonia (NH_3) is taken up as N-source by the phototrophs and the nitrifiers. It is also used as a reactant in the catabolism of nitrifiers, where it is eventually converted into nitrate. Ammonia is furthermore formed from the decay and lysis of microbial matter, as well as from hydrolysis of particulate organic material. The ammonium ion (NH_4^+) is formed from the pH-dependent acid–base equilibrium of dissolved ammonia. At pH values below nine, ammonium is the dominant species, and above that value the equilibrium shifts to ammonia. Nitrate (NO_3^-) is used as alternative N-source by the phototrophs (Dortch, 1990) as well as electron acceptor by denitrifying heterotrophs.

S_H, S_{cat}, S_{an} (kmol m^{-3}): Hydrogen Ion, Cations, and Anions

The concentration of the hydrogen ion is included in the model in order to enable pH calculation. It is calculated algebraically from the charge balance. Anions and cations are considered to be non-reactive. They are added into the system for charge compensation through a pH setpoint control algorithm.

References

Bader FG. 1978. Analysis of double-substrate limited growth. Biotechnol Bioeng 20(2):183–202.

Barbosa MJ, Janssen M, Ham N, Tramper J, Wijffels RH. 2003. Microalgae cultivation in air-lift reactors: Modeling biomass yield and growth rate as a function of mixing frequency. Biotechnol Bioeng 82(2):170–179.

Cloot AHJ, Pieterse AJH. 1999. Modelling phytoplankton in the Vaal River (South Africa). Water Sci Technol 40(10):119–124.

Dircks K, Henze M, van Loosdrecht MCM, Mosbaek H, Aspegren H. 2001. Storage and degradation of poly-beta-hydroxybutyrate in activated sludge under aerobic conditions. Water Res 35(9):2277–2285.

Dortch Q. 1990. The interaction between ammonium and nitrate uptake in phytoplankton. Mar Ecol-Progr Ser 61(1–2):183–201.

dosSantos VAPM, Marchal LM, Tramper J, Wijffels RH. 1996. Modeling and evaluation of an integrated nitrogen removal system with micro-organisms co-immobilized in double-layer gel beads. Biotechnol Progr 12(2):240–248.

Duarte P, Ferreira JG. 1997. Dynamic modelling of photosynthesis in marine and estuarine ecosystems. Environ Modell Assess 2:83–93.

Ebrahimi S, Picioreanu C, Kleerebezem R, Heijnen JJ, van Loosdrecht MCM. 2003. Rate-based modelling of SO_2 absorption into aqueous $NaHCO_3/Na_2$ CO_3. solutions accompanied by the desorption ofCO_2. Chem Eng Sci 58(16):3589–3600.

Eilers PHC, Peeters JCH. 1988. A model for the relationship between Light-Intensity and the rate of photosynthesis in Phytoplankton. Ecol Model 42(3–4):199–215.

Eppley RW, Rogers JN, McCarthy JJ. 1969. Half-saturation constants for uptake of nitrate and ammonium by marine phytoplankton. Limnol Oceanogr 14(6):912–920.

Falkowski PG, Wirick CD. 1981. A simulation-model of the effects of vertical mixing on primary productivity. Mar Biol 65(1):69–75.

Falkowski PG, Dubinsky Z, Wyman K. 1985. Growth-Irradiance Relationships in Phytoplankton. Limnol Oceanogr 30(2):311–321.

Flora JRV, Suidan MT, Biswas P, Sayles GD. 1995. Modeling algal biofilms—Role of carbon, light, cell-surface charge, and ionic species. Water Environ Res 67(1):87–94.

Geesey G, Jang L. 1990. Extracellular polymers for metal binding. In: Brierley CL, editors. Microbial mineral recovery. New York: McGraw-Hill. p 223–247.

Goldman JC. 1999. Inorganic carbon availability and the growth of large marine diatoms. Mar Ecol-Progr Ser 180:81–91.

Gregoire M, Soetaert K, Nezlin N, Kostianoy A. 2004. Modeling the nitrogen cycling and plankton productivity in the Black Sea using a three-dimensional interdisciplinary model. J Geophys Res 109(C05007): doi:10.1029/2001JC001014.

Henze M, Gujer W, Mino T, van Loosdrecht M. 2000. Activated sludge models ASM1, ASM2, ASM2D and ASM3. London: IWA Publishing.

Horn H, Hempel DC. 1997. Growth and decay in an auto-/heterotrophic biofilm. Water Res 31(9):2243–2252.

Horn H, Neu TR, Wulkow M. 2001. Modelling the structure and function of extracellular polymeric substances in biofilms with new numerical techniques. Water Sci Technol 43(6):121–127.

Huisman J, van Oostveen P, Weissing FJ. 1999. Species dynamics in phytoplankton blooms: Incomplete mixing and competition for light. Amer Naturalist 154(1):46–68.

Jupsin H, Praet E, Vasel JL. 2003. Dynamic mathematical model of high rate algal ponds (HRAP). Water Sci Technol 48(2):197–204.

Kirk JTO. 1994. Light and photosynthesis in aquatic ecosystems. Cambridge, UK: Cambridge University Press.

Kromkamp J. 1987. Formation and functional-significance of storage products in cyanobacteria. N Z J Mar Freshwater Res 21(3):457–465.

Mankad T, Nauman EB. 1992. Modeling of microbial-growth under dual limitations. Chem Eng J Biochem Eng J 48(2):B9–B11.

Merrick JM. 1978. Metabolism of reserve materials. In: Sistrom WR, editors. The photosynthetic bacteria. New York, USA: Plenum Press. p 199–219.

Morris EP, Kromkamp JC. 2003. Influence of temperature on the relationship between oxygen- and fluorescence-based estimates of photosynthetic parameters in a marine benthic diatom (Cylindrotheca closterium). Euro J Physcol 38(2):133–142.

Musvoto EV, Wentzel MC, Loewenthal RE, Ekama GA. 2000. Integrated chemical-physical processes modelling-I. Development of a kinetic-based model for mixed weak acid/base systems. Water Res 34(6):1857–1867.

Neu TR, Lawrence JR. 1997. Development and structure of microbial biofilms in river water studied by confocal laser scanning microscopy. FEMS Microbiol Ecol 24(1):11–25.

Pahl-Wostl C. 1992. Dynamic versus static models for photosynthesis. Hydrobiologia 238:189–196.

Picioreanu C, vanLoosdrecht MCM, Heijnen JJ. 1997. Modelling the effect of oxygen concentration on nitrite accumulation in a biofilm airlift suspension reactor. Water Sci Technol 36(1):147–156.

Reichert P. 1998. AQUASIM. Version 2.0. Dübendorf. Switzerland: Swiss Federal Institute for Environmental Science and Technology (EAWAG).

Reichert P. 2001. River water quality Model no. 1 (RWQM1): Case study II. Oxygen and nitrogen conversion processes in the River Glatt (Switzerland). Water Sci Technol 43(5):51–60.

Reichert P, Borchardt D, Henze M, Rauch W, Shanahan P, Somlybody L, Vanrolleghem PA. 2001. River water quality Model No. 1. London: IWA Publishing. Report nr 12.

Roeselers G, Zippel B, Staal M, van Loosdrecht MCM, Muyzer G. 2006. On the reproducibility of microcosm experiments—Different community composition in parallel phototrophic biofilm microcosms. FEMS Microbiol Ecol 58(2):169–178.

Ryder DN, Sinclair CG. 1972. Model for growth of aerobic microorganisms under oxygen limiting conditions. Biotechnol Bioeng 14(5):787–798.

Schumacher G, Sekoulov I. 2003. Improving the effluent of small wastewater treatment plants by bacteria reduction and nutrient removal with an algal biofilm. Water Sci Technol 48(2):373–380.

Sirevag R, Ormerod JG. 1977. Synthesis, storage and degradation of polyglucose in chlorobium-thiosulfatophilum. Arch Microbiol 111(3):239–244.

Smith AJ. 1983. Modes of cyanobacterial carbon metabolism. Ann Microbiol B 134(1):93–113.

Smith DJ, Underwood GJC. 2000. The production of extracellular carbohydrates by estuarine benthic diatoms: The effects of growth phase and light and dark treatment. J Phycol 36(2):321–333.

Staal M, Thar R, Kühl M, van Loosdrecht MCM, Wolf G, de Brouwer JFC, Rijstenbil JW. 2007. Carbon isotope fractionation in developing natural phototrophic biofilms. Biogeosciences Discussions 4:69–98.

Stal LJ. 2003. Microphytobenthos, their extracellular polymeric substances, and the morphogenesis of intertidal sediments. Geomicrobiol J 20(5):463–478.

Thorud M, Sirevag R. 1982. Kinetics of polyglucose breakdown in chlorobium. Arch Microbiol 133(2):114–117.

Tillmann U, Rick H-J. 2001. Synthesis and new conception of north sea research (SYCON). Working group 7: Phytoplankton. Hamburg: Universität Hamburg. Report nr 9.

van Dam AA, Beveridge MCM, Azim ME, Verdegem MCJ. 2002. The potential of fish production based on periphyton. Rev Fish Biol Fisheries 12(1):1–31.

van Loosdrecht MCM, Pot MA, Heijnen JJ. 1997. Importance of bacterial storage polymers in bioprocesses. Water Sci Technol 35(1):41–47.

Varela RA, Cruzado A, Gabaldon JE. 1995. Modeling primary production in the North-Sea using the European-Regional-Seas-Ecosystem-Model. Neth J Sea Res 33(3–4):337–361.

Wanner O, Gujer W. 1986. A multispecies biofilm model. Biotechnol Bioeng 28(3):314–328.

Wanner O, Reichert P. 1996. Mathematical modeling of mixed-culture biofilms. Biotechnol Bioeng 49(2):172–184.

Wiesmann U. 1994. Biological nitrogen removal from wastewater. In: Fiechtner A, editors. Advances in biochemical engineering/biotechnology. Berlin, Germany: Springer-Verlag. p 113–154.

Wu XX, Merchuk JC. 2002. Simulation of algae growth in a bench-scale bubble column reactor. Biotechnol Bioeng 80(2):156–168.

Zimmo OR, van der Steen NP, Gijzen HJ. 2004. Nitrogen mass balance across pilot-scale algae and duckweed-based wastewater stabilisation ponds. Water Res 38(4):913–920.

Zippel B, Neu TR. 2005. Growth and structure off phototrophic biofilms under controlled light conditions. Water Sci Technol 52(7):203–209.

Zonneveld C. 1998. Photoinhibition as affected by photoacclimation in phytoplankton: A model approach. J Theor Biol 193(1):115–123.